WEP Warwick Evans Publishing

International Journal of Electric Power and Energy Studies

ISSN: 3006-2004 (Print), ISSN: 3006-0826 (Online) | Volume 2, Number 1, Year 2024
DOI: https://doi.org/10.62051/ijepes.v2n1.09
Journal homepage: https://wepub.org/index.php/IJEPES/index

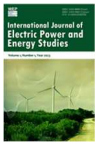

# Achieving High Energy Storage Performance in Lead-Free Relaxor Ferroelectric Ceramics of (1-*x*)$Bi_{0.88}Nd_{0.10}Sm_{0.02}FeO_3$-x$BaTiO_3$

Houren Wei*, Zaiwen Yang

College of Physics and Electronic Information, Henan Polytechnic University, Jiaozuo 454000, China

*Corresponding Author: Houren Wei

## ABSTRACT

$BiFeO_3$-based lead-free ferroelectrics have attracted great interest in energy storage applications due to their high spontaneous polarisation strength, however, the high residual polarisation strength ($P_r$) has become a serious obstacle to their practical application. In this work, (1-*x*)$Bi_{0.88}Nd_{0.10}Sm_{0.02}FeO_3$-x$BaTiO_3$+0.1 wt% $MnO_2$ ceramics were designed by ion doping and solid solution modification strategies, where $Sm^{3+}$ and $Nd^{3+}$ promote ionic disorder and reduce leakage current, and the introduction of nano-$BaTiO_3$ induces the crushing of long-range ferroelectric structure into polar nano-regions with enhanced relaxation. As a result, the ceramic is able to maintain a high maximum polarisation intensity while possessing a low residual polarisation.The recoverable energy density ($W_{rec}$) of the 0.50BSNF-0.50BT ceramic is as high as 3.61 J/cm$^3$ with an efficiency of 70.11%. In addition, the 0.50BSNF-0.50BT has good thermal stability ($W_{rec}$ variation <7%) at 25-120°C. In the charge/discharge test, the $W_{dis}$ was 2.58 J/cm$^3$ and the discharge time was 273 ns. These results indicate that the 0.50BSNF-0.50BT ceramic is an ideal candidate as a material for energy storage applications.

## KEYWORDS

$BiFeO_3$ Ceramics; Relaxor Ferroelectric Ceramics; Energy Storage; Nanocluster Structure; Storage Efficiency.

## 1. INTRODUCTION

Facing the urgent challenges of global environmental protection and sustainable development, the research and development of green and efficient energy storage technologies has become one of the hot spots in the field of scientific research[1,2]. Among today's diverse energy storage technologies, dielectric capacitors are attracting more and more attention due to their extraordinary power density and excellent fast charging and discharging capabilities, showing great potential in high-tech applications such as LIDAR systems, high-speed electronic communication infrastructures, and new energy vehicles[3]. The energy storage density of a dielectric capacitor is usually calculated from the *P-E* curve by the following series of equations[4,5]:

$$W_{total} = \int_0^{P_{max}} EdP \tag{1}$$

$$W_{rec} = \int_{P_r}^{P_{max}} EdP \tag{2}$$

$$\eta = \frac{W_{rec}}{W_{total}} \times 100\% \tag{3}$$

where $W_{total}$ and $W_{rec}$ denote the total energy density and effective energy storage density during charging, respectively, $P_{max}$ is the maximum polarisation, $P_r$ is the residual polarisation, $\eta$ is the energy storage efficiency, and $E$ is the electric field. Obviously, a large difference between high dielectric breakdown strength ($E_b$) and $\Delta P$ ($\Delta P=P_{max}-P_r$) is necessary to achieve high $W_{rec}$[6]. According to the different characteristics of *P-E* curves, ceramic energy storage materials can be classified into four categories: linear dielectrics (LDs), normal ferroelectrics (FEs), relaxation ferroelectrics (RFEs), and antiferroelectrics (AFEs)[7,8]. Linear dielectrics are characterised by zero $P_r$ and high $E_b$, but the small polarisation limits their energy storage density. Typical FEs have significant $P_{max}$ but are limited by their relatively poor $W_{rec}$, $\eta$, and $E_b$. antiferroelectrics exhibit double hysteresis loops with higher $W_{rec}$ but lower $\eta$ and poor temperature stability[9]. Therefore, relaxation ferroelectrics with higher $P_{max}$ and lower $P_r$ have received significant attention for energy storage applications.

In recent years, several lead-free $ABO_3$ chalcogenide-structured relaxing ferroelectric ceramics, $BaTiO_3$ (BT), modified $(Bi_{0.5}Na_{0.5})TiO_3$ (BNT) and $(K_{0.5}Na_{0.5})NbO_3$ (KNN), have been extensively investigated in order to replace widely used Pb-based relaxing ferroelectric ceramics, taking into account environmental protection issues, and have achieved a great improvement in energy storage performance[10-12]. However, it is difficult to obtain both high $W_{rec}$ (>2 J/cm$^3$) and efficiency ($\eta$ >70%) for most Pb-free ceramics[13]. Bismuth ferrate ($BiFeO_3$,BF) is a promising candidate for lead-free ceramics due to the unique $6s^2$ isolated electron pair structure of $Bi^{3+}$ ions, with spontaneous polarisation strengths up to ~100 μC/cm²[14]. Although its energy storage application is limited by large $P_r$, it can be optimised by doping modification. Barium titanate ($BaTiO_3$,BT) has moderate $P_{max}$ and low $P_r$. Li[15] proposed that the structural evolution of $BiFeO_3$-$BaTiO_3$ (BF-BT) solid solution exhibits the coexistence of two phases, and shows excellent saturation polarization strength near the quasi-isotropic phase boundary (MPB), so modification studies based on the BF-BT material are highly favoured in the field of energy storage .Zhu[16] et al. showed the modification of BF-BT material by adding a dopant to the $0.52BiFeO_3$-$0.48BaTiO_3$ ceramics modified by adding $La_2O_3$ and $MnO_2$, which effectively enhanced the Eb of the material, with $W_{rec}$ of 1.22 J/cm$^3$ and $\eta$ of 58% at 140 kV/cm $E_b$. Liu[17] et al. designed $0.6BiFeO_3$-$0.48BaTiO_3$ ceramics by introducing $Ba(Zn_{1/3}Ta_{2/3})O_3$ (BZT) into BF-based ceramics. In order to inhibit the formation of long-range ordered structures, $BiFeO_3$-$0.34BaTiO_3$-$0.06Ba(Zn_{1/3}Ta_{2/3})O_3$ composite ceramic structures were constructed by constructing random fields. Under an electric field of 160 kV/cm, the $W_{rec}$ was 2.56 J/cm$^3$ and the $\eta$ was 71%.Wang[18] et al. achieved a $W_{rec}$ of 2.56 J/cm$^3$ and an $\eta$ of 71% when they doped Nd into a 0.75 $(Bi_{1-x}Nd_x)$ $FeO_3$-$0.25BaTiO_3$ composite system, a $W_{rec}$ of up to 1.82 J/cm³ was obtained at 180 kV/cm $E_b$, indicating that rare-earth doping can effectively modulate the storage performance of BF-BT solid solutions.

In this study, rare earth ions $Nd^{3+}$ and $Sm^{3+}$ doping were introduced to overcome the defect of high leakage current of pure BF and promote the formation of random field and stress field inside the ceramics, meanwhile, nano-$BaTiO_3$ was added to form a solid solution, and the long-range ordered ferroelectric domains were transformed into short-range ordered nano domains or polar nano-regions, which further reduced the value of $P_r$ and obtained a high $W_{rec}$. In addition, the ceramics were added with a small amount (0.1 wt%) of $MnO_2$ was added to the ceramics to further reduce the leakage current. The results show that all the samples ($x$=0.33-0.55) have a pure chalcogenide structure and a dense microstructure. high $W_{rec}$ of 3.61 J/cm$^3$ and high $\eta$ of 70.11% were achieved at $x$=0.50 under

an electric field of 280 kV/cm. Meanwhile, the ceramics exhibit good thermal stability (25-120°C) and excellent charge/discharge performance. These results indicate that (1-*x*)BSNF-*x*BT ceramics have a promising future for energy storage devices.

## 2. EXPERIMENTAL SECTION

(1-*x*)$Bi_{0.88}Nd_{0.10}Sm_{0.02}FeO_3$-*x*$BaTiO_3$+0.1 wt% $MnO_2$ ceramics (referred to as (1-*x*)BSNF-*x*BT ceramics, *x*=0.33, 0.42, 0.50, 0.55) were prepared by the solid phase method. The main raw materials were $Bi_2O_3$ (99.5%), $Fe_2O_3$ (99.5%), $Nd_2O_3$ (99.9%), nano-$BaTiO_3$ (99.9%), $Sm_2O_3$ (99.9%) and $MnO_2$ (98%). The raw material powders were weighed according to the stoichiometric ratio and ball-milled with $ZrO_2$ balls in ethanol for 24 h. After drying, they were calcined for 5 h at 750°C. After calcination, a small amount (0.1 wt%) of $MnO_2$ was added to imP$_r$ove electrical insulation and ball-milled again with anhydrous ethanol and zirconia balls for 24 h. 8 wt% polyvinyl alcohol solution (PVA) was added dropwise and pressed to form discs of about 10 mm diameter. To remove the PVA from the samples, the samples were sintered at 550°C for 1 h and then at 860-940°C for 3 h.

The phase structure and microstructure were investigated by X-ray diffraction (PANalytical X′Pert Pro, The Netherlands) and scanning electron microscopy (Merlin Compact, Germany), and Raman spectroscopy was carried out using a Raman spectrometer (LabRAM HR, Horiba Corporation, Japan) with an excitation source of 514 nm. a A ferroelectric tester (Radiant Technologies Inc. precision P$_r$emier II, USA) was used to test the hysteresis loop (*P*-*E*). The dielectric temperature spectrum was tested by a dielectric temperature spectrum test system (DMS-2000, China). Charge/discharge performance was tested by charge/discharge test system (GT-002, China).

## 3. RESULTS AND DISCUSSION

Fig. 1(a) shows the X-ray diffraction patterns of (1-*x*)BSNF-xBT ceramic samples with different $BaTiO_3$ contents. From the figure, it can be clearly observed that all the prepared (1-*x*)BSNF-*x*BT ceramics are of chalcogenide structure with no heterogeneous phases generated, which indicates the successful doping of Nd, Sm, and nano-$BaTiO_3$ into the $BiFeO_3$ matrix lattice. The (200) diffraction peak region was magnified locally as shown in Fig. 1(b). The results show that the (200) diffraction peak gradually shifted to a lower angle with the increase of the $BaTiO_3$ fraction, indicating that the lattice was slightly expanded due to the substitution of $Bi^{3+}$ (~1.03 Å) by $Ba^{2+}$ (~1.35 Å), which has a larger ionic radius, in the A-site. The (200) splitting peak at *x*=0.33 indicates that the 0.67BSNF-0.33BT ceramic The existence of two phases, orthorhombic and pseudocubic, coexisted, and the (200) splitting peak shifted to an asymmetric single peak as the BT doping increased, indicating that the ceramic structure shifted from an orthorhombic phase to a pseudocubic phase[19,20]. In order to explain the lattice expansion effect more accurately, the lattice constants a, b and c of different samples were calculated with the help of Jade software, and the results are shown in Table 1. Comparative analysis of the data reveals that the corresponding three lattice constants a, b and c show an increasing trend with the increase of $BaTiO_3$ content, which further confirms that the lattice expansion induced by doping $BaTiO_3$.

To further illustrate the effect of BT incorporation on the ceramic structure, Figure 1(c) shows the Raman spectra of (1-*x*)BSNF-xBT ceramics.The Raman peaks near 280 $cm^{-1}$ broaden with increasing BT content, probably due to the doping of ions with different ionic radii and different valence states, which leads to the disorder and structural complexity of the A-site cation Increase. The wavelength changes from 280 $cm^{-1}$ to 296 $cm^{-1}$ with increasing BT content, reflecting the weakening of the B-O bond and the transition of the system to the relaxed ferroelectric state[21]. The Raman mode broadens at 400-600 $cm^{-1}$ when *x*<0.55, indicating that the increase in the nano-$BaTiO_3$ content leads to an increase in the disorder of the system and the formation of PNRs, and the peaks become sharp when

the *x* content is further increased, which can be attributed to a decrease in the degree of disorder, and this evolution coincides with the energy storage properties of the ceramics discussed later[22].

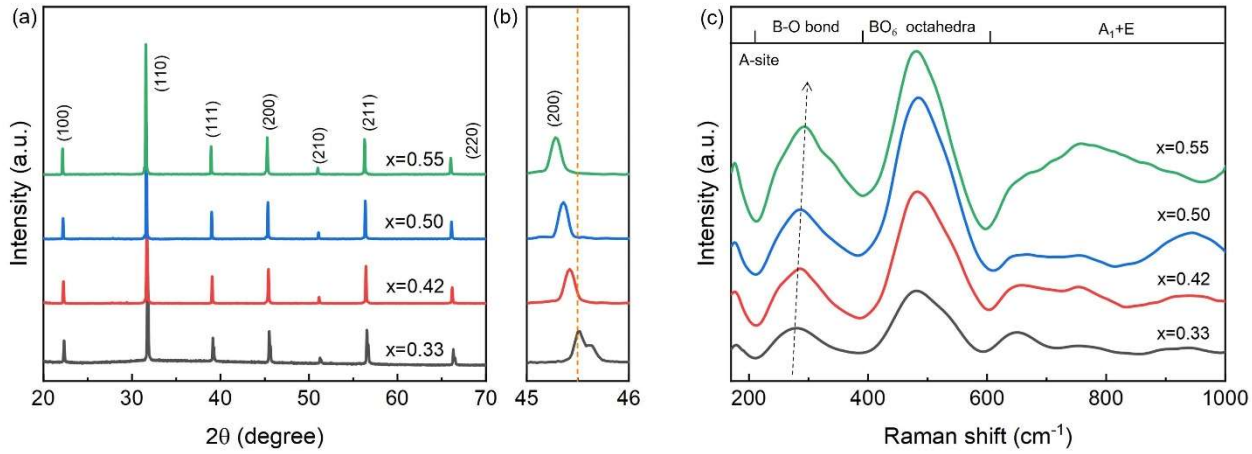


**Fig. 1** (a) XRD patterns of (1-x)BSNF-xBT ceramics at 20-70° and (b) 45-46°. (c) Raman spectra of (1-x)BSNF-xBT ceramics at room temperature

**Table 1.** Lattice constants of (1-x)BSNF-xBT ceramics

| *x* | a | b | c |
|---|---|---|---|
| 0.33 | 3.9831 | 3.9831 | 3.9831 |
| 0.42 | 3.9905 | 3.9905 | 3.9905 |
| 0.50 | 3.9953 | 3.9953 | 3.9953 |
| 0.55 | 3.9972 | 3.9972 | 3.9972 |

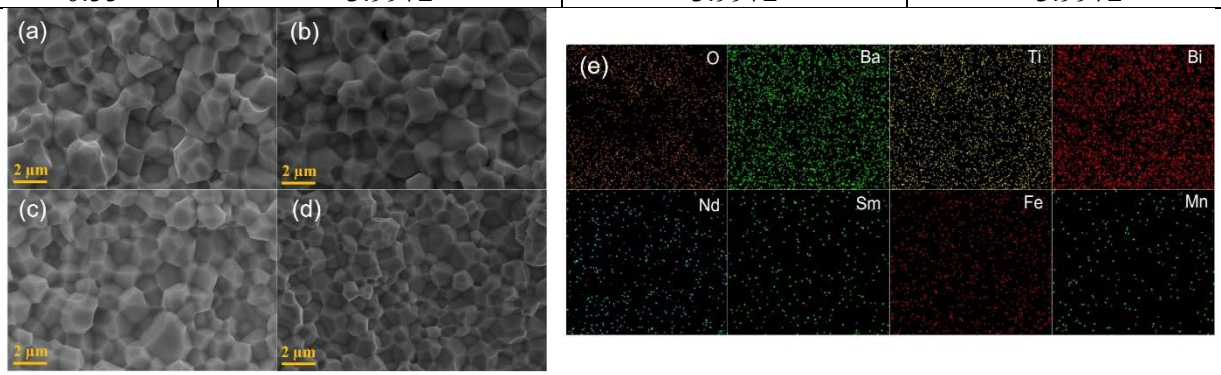


**Fig. 2** microstructural images of the surface of (1-x)BSNF-xBT ceramics (a) x=0.33, (b) x=0.42, (c) x=0.50, (d) x=0.55, (e) Elemental mapping distributions of 0.50 BSNF-0.50 BT ceramics

Fig. 2(a)-(d) shows the scanning electron microscope (SEM) images of (1-*x*)BSNF-*x*BT ceramic samples with different $BaTiO_3$ contents. It can be clearly seen that all the samples have uniform grain size with obvious grain boundaries and dense microstructure. Fig. 2(e) shows the elemental mapping distribution of 0.50BSNF-0.50BT ceramics, and the images indicate that the elements of Bi, Ba, Ti, Fe, Nd, Sm, Mn, and O are uniformly distributed without elemental enrichment and segregation, and the uniform elemental distribution is conducive to the obtaining of stable electrical properties. When the BT content was increased from 0.33 to 0.55, the grain size decreased from the original 2.17 μm to 1.56 μm, reflecting a significant grain refinement effect, as shown in Fig. 3 (a)-(d). The decrease in grain size can be explained by the gradual decrease in the concentration of volatile ions Bi with the increase in BT content, leading to a decrease in the concentration of oxygen vacancies, which inhibits mass transfer[23,24].

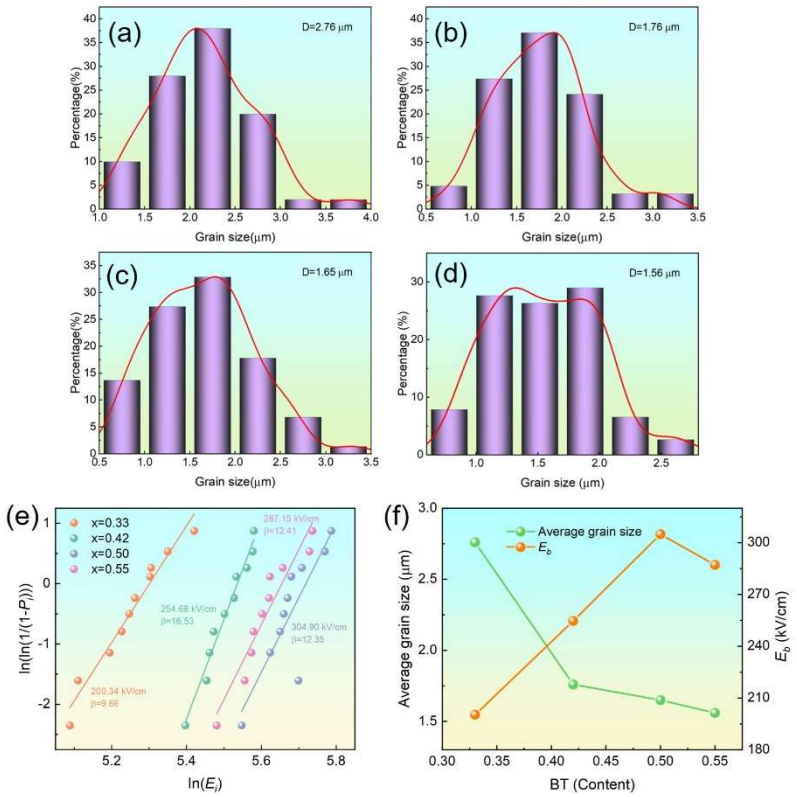


**Fig. 3** Grain size distribution of (1-x) BSNF-xBT ceramics: (a) x=0.33, (b) x=0.42, (c) x=0.50, (d) x=0.55, (e) Weibull distribution, and (f) average grain sizes and Eb values of different BT doping

The breakdown electric field of (1-*x*)BSNF-*x*BT ceramics was analysed using the Weibull statistical method, as shown in Fig. 3(e). The relevant calculation formula is as follows[25]: $X_i=\ln(E_i)$,$Y_i=\ln(\ln(1/(1-P_i)))$, where i is the number of the sample, $E_i$ is the breakdown electric field of the sample numbered i, and n is the total number of samples. It can be observed that all the experimental data points show a good linear relationship with a slope greater than 9, which reflects the high reliability and consistency of the obtained data. With the increase of $BaTiO_3$ content, the average breakdown electric field, $E_b$, of the ceramic materials generally shows an increasing trend from 200.34 kV/cm at $x$=0.33 to 304.90 kV/cm at $x$= 0.50, followed by a slight decrease. Figure 3(f) shows that the breakdown electric field tends to increase as the grain size decreases. The decrease in grain size implies an increase in the number of grain boundaries per unit volume. The presence of grain boundaries can effectively hinder the internal charge migration and help to improve the breakdown strength of ceramic materials[26]. When $x$>0.50, a slight decrease in the electric field strength occurs, which is due to the fact that $E_b$ is affected by factors such as porosity, relative density and defects in addition to grain size[27].

Figs 4(a)-(d) show the dielectric properties of (1-*x*)BSNF-*x*BT ceramics. With the increase of frequency, the dielectric constant peak broadens and moves to the high temperature direction, and the $\varepsilon_r$ value gradually decreases, showing obvious characteristics of frequency dispersion and diffuse phase transition[28]. With the increase of BT, $\varepsilon_r$ decreases steadily, and a wide peak plateau appears between the non-traversed relaxation states and the traversed relaxation states. The $\varepsilon_r$ curve becomes flat in the temperature range of 0-200°C, revealing that the enhancement of relaxation behaviours and the long-range ordering of ferroelectrics are damaged, which is conducive to inducing more traversed relaxation states, which prompts the transformation of the large ferroelectric domains into PNRs, and thus reduces the $P_r$ and improves the energy storage performance. In addition, the flat $\varepsilon_r$ curve over a wide temperature range indicates that the temperature stability of (1-*x*)BSNF-xBT ceramics is improved with the addition of BT. At lower temperatures, the tanδ values of all ceramics remain small, indicating that the leakage current is reduced after the incorporation of BT. tanδ gradually increases

with the increase of temperature, which may be due to the increase of leakage current due to the increase of defects at high temperature[29].

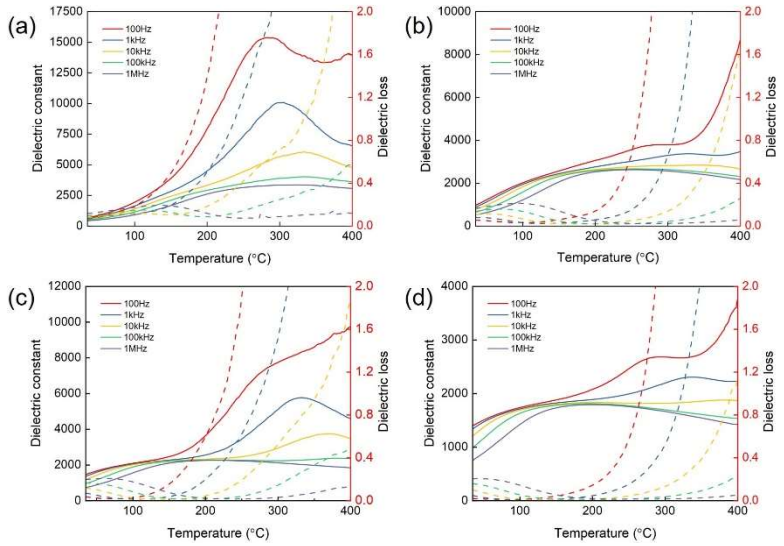


**Fig. 4** Dielectric properties and losses of (1-x) BSNF-xBT ceramics with temperature (a) x=0.33, (b) x=0.42, (c) x=0.50, (d) x=0.55

The ferroelectric properties of the ceramics can be visualised by the *P-E* curve. From Fig. 5(a), it can be seen that at $x$=0.33, the curve exhibits a fatter, with a large polarisation intensity as well as a high residual polarisation intensity, and a strong ferroelectricity. With the increase of BT doping, the relaxation is enhanced and the polarisation intensity decreases from 47.60 kV/cm to 23.82 kV/cm, and $P_r$ also decreases from 13.90 μC/cm$^2$ to 2.06 μC/cm$^2$, and the *P-E* curve is refined. The corresponding change in energy storage performance is calculated as shown in Fig. 5(b). When the BT doping increases, the energy storage density decreases due to the decrease in polarisation strength, while the significant decrease in $P_r$ leads to the increase of $\eta$ to about 80%. The bipolar *P-E* curves of (1-$x$)BSNF-$x$BT ceramics at maximum electric field are shown in Fig. 5(c), and the corresponding energy storage density and efficiency variations with BT content are shown in Fig. 5(d). As the BT doping content increases, $\eta$ gradually increases while the ceramic material shows higher $E_b$ and delayed polarisation saturation. When $x$=0.50, the (1-$x$)BSNF-$x$BT obtains a maximum breakdown electric field of 280 kV/cm and maintains a high saturation polarisation intensity of 41.13 μC/cm², and the residual polarisation decreases to 5.76 μC/cm², meanwhile, the $W_{rec}$ reaches 3.61 J/cm³, which corresponds to an energy storage efficiency of $\eta$ of 70.11%, which sufficiently demonstrates that the material has better energy storage characteristics. When the doping ratio exceeds $x$=0.50, the lower $P_m$ leads to a subsequent decrease in the energy storage density $W_{rec}$.

The 0.50BSNF-0.50BT ceramic system, which exhibits the best energy storage performance, was further investigated. It can be seen in Fig. 6(a) that $P_m$ increases significantly with increasing electric field strength while $P_r$ is maintained at a low level, and all curves have a slender shape due to the excellent relaxation properties. Fig. 6(b) shows that the energy storage density increases with the enhancement of the electric field strength, and the energy storage efficiency $\eta$ of the 0.50BSNF-0.50BT ceramics is consistently above 70%, which is attributed to the formation of PNRs that make the polarisation flip easier, while grain refinement promotes the $E_b$ increase[30,31]. The ambient temperature has a significant impact on the performance of electronic devices and energy storage materials, so excellent temperature stability of energy storage materials is important.

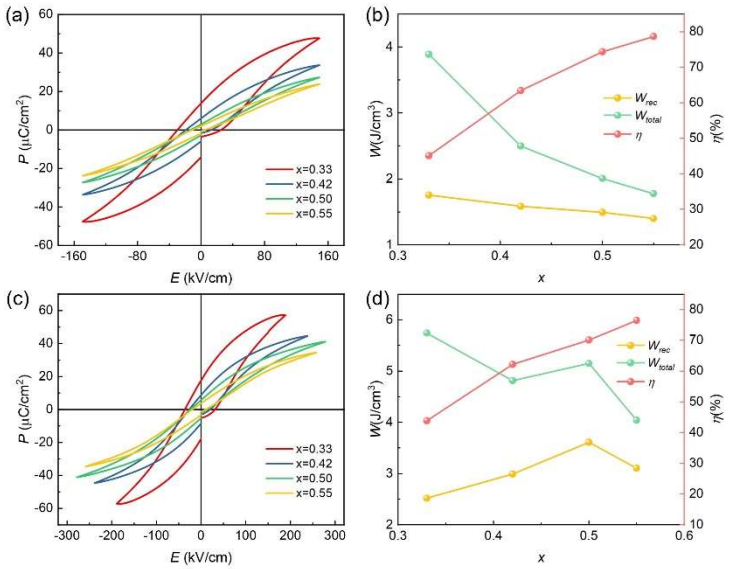


**Fig. 5** (a) Room temperature bipolar P-E curves of (1-x) BSNF-xBT ceramics under 150 kV/cm electric field, (b) corresponding energy storage density and efficiency, (c) room temperature bipolar P-E curves of (1-x) BSNF-xBT ceramics under the maximum electric field and corresponding (d) energy storage density and efficiency

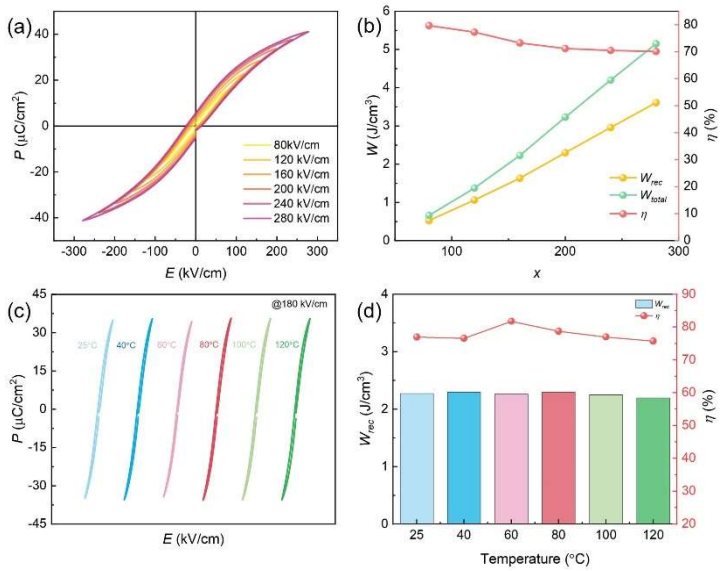


**Fig. 6** (a) Bipolar P-E curves of 0.50BSNF-0.50BT ceramics at different electric fields, (b) corresponding energy storage density and efficiency, (c) P-E curves of x=0.50 samples at different temperatures under 180 kV/cm electric field, (d) corresponding changes in η and Wrec values with temperature

Fig. 6(c) shows that the 0.50BSNF-0.50BT ceramic $P_r$ is increased by enhanced ionic conduction and increased leakage current as the temperature increases from room temperature to 120°C, but still maintains the shape of the elongated *P-E* curve. Meanwhile, it is shown in Fig. 6(d) that $W_{rec}$ slightly decreases from 2.31 J/cm³ to 2.20 J/cm³ with increasing temperature, and the overall change is less than 7%. The above results show that the ceramic material can still maintain good storage performance at higher temperatures, reflecting the excellent temperature stability of the 0.50BSNF-0.50BT energy storage ceramic.

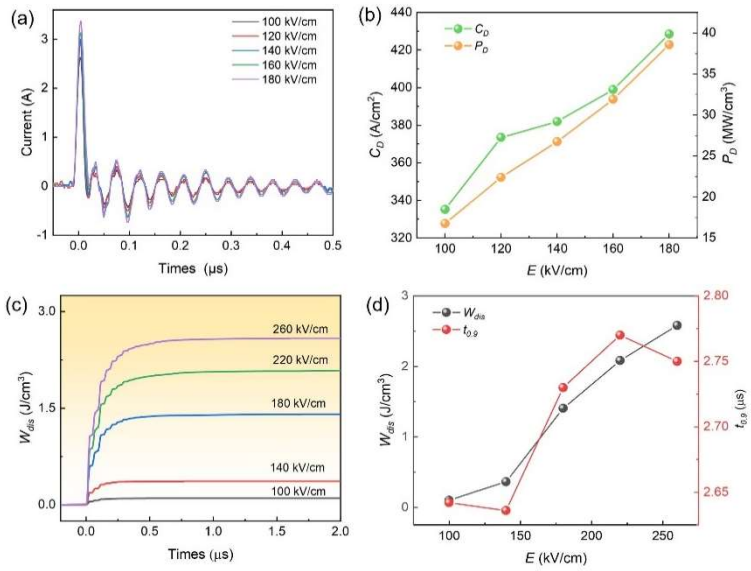


**Fig. 7** (a) The underdamped discharge current density curve of 0.50BSNF-0.50BT sample under different electric fields; (b) the relationship between PD and CD and electric field; (c) the relationship between Wdis and time; (d) the changes of Wdis and t0.9 values with applied electric field

In order to evaluate the performance of the capacitors for practical applications, the charging and discharging performance of the 0.50BSNF-0.50BT ceramics was tested[32]. (Underdamped discharge current density curves for Fig. 7(a). As the electric field strength increases, the peak current increases from 2.63 A at 100 kV/cm electric field to 3.37 A at 180 kV/cm. From Fig. 7(b), it can be seen that both the discharge current density ($C_D = I_{max}/S$) and the discharge power density ($P_D = E \times I_{max}/S$, S refers to the electrode area) increase with the increase of the electric field and reach the 180 kV/cm maximum value ($C_D$=428.57 A/cm$^2$, $P_D$=38.58 MW/cm$^3$). The ceramics were tested for overdamped discharge with a load resistance of 1634 Ω. Figure 7(c) shows that when the electric field rises from 100 kV/cm to 260 kV/cm, The discharge energy density ($W_{dis} = \frac{R\int I^2(t)dt}{V}$) increased from 0.10 J/cm$^3$ to 2.58 J/cm$^3$ , reaching the highest value in a very short time. $W_{dis}$ slightly smaller than $W_{rec}$ calculated from the *P-E* curve for the same electric field, and this difference may be attributed to the fact that the loading frequency during charging and discharging is much higher than that during the measurement of the *P-E* return line . Usually $t_{0.9}$ is regarded as the time to release 90% of the discharged energy, and Fig. 7(d) shows that with the increase of electric field $W_{dis}$ and $t_{0.9}$ show an overall increasing trend, and $t_{0.9}$ is about 273 ns for 0.50BSNF-0.50BT ceramics under an electric field of 260 kV/cm. Taken together, the above data indicate that 0.50BSNF-0.50BT ceramics have excellent charge-discharge performance, and the application prospect is broad.

## 4. CONCLUSION

Lead-free (1-*x*)BSNF-*x*BT relaxation ferroelectric ceramics were successfully prepared by solid-phase method. The pseudo-cubic phase chalcogenide structure was confirmed by XRD. The introduction of rare earth elements Sm and Nd reduced the leakage current and promoted the ionic disorder, and the solid solution of nano-BT induced the generation of polar nano-regions and enhanced the relaxation behaviour. By improving the endogenous and exogenous factors (microstructure, average grain size), the 0.50BSNF-0.50BT ceramics obtained a high $W_{rec}$ of 3.61 J/cm$^3$ and a high efficiency of 70.11% at 280 kV/cm. In addition, the 0.50BSNF-0.50BT ceramic maintains excellent stability in the temperature interval of 25-120°C, along with impressive $C_D$ (857.31 A/cm$^2$) and $P_D$ (94.25 MW/cm3) at an electric field of 220 kV/cm, and a significant enhancement of the $W_{dis}$ up to 2.58 J/cm³ at 360 kV/cm. $t_{0.9}$ of 273 ns, indicating the excellent

charge/discharge performance of the material. These results indicate that 0.50BSNF-0.50BT ceramics are a potential alternative material for energy storage.

## REFERENCES


[1] Yang L, Kong X, Li F, Hao H, Cheng Z, Liu H, Li J-F, Zhang S. Perovskite lead-free dielectrics for energy storage applications[J].Progress in Materials Science,2019, 102: 72-108.

[2] Wang G, Lu Z, Li Y, Li L, Ji H, Feteira A, Zhou D, Wang D, Zhang S, Reaney I M. Electroceramics for High-Energy Density Capacitors: Current Status and Future Perspectives[J].Chemical Reviews,2021, 121 (10): 6124-6172.

[3] Zhang H, Wei T, Zhang Q, Ma W, Fan P, Salamon D, Zhang S-T, Nan B, Tan H, Ye Z-G. A review on the development of lead-free ferroelectric energy-storage ceramics and multilayer capacitors[J].Journal of Materials Chemistry C,2020, 8 (47): 16648-16667.

[4] Hu D, Pan Z, Zhang X, Ye H, He Z, Wang M, Xing S, Zhai J, Fu Q, Liu J. Greatly enhanced discharge energy density and efficiency of novel relaxation ferroelectric BNT–BKT-based ceramics[J].Journal of Materials Chemistry C,2020, 8 (2): 591-601.

[5] Chen C S, Lin Z Q, Montecillo R. Improved energy storage in antiferroelectric AgNbO3-modulated 0.925Bi(0.5)Na(0.5)TiO3-0.075BaTiO3 relaxor ferroelectric ceramic[J].CERAMICS INTERNATIONAL,2022.

[6] Gao X, Li Y, Chen J, Yuan C, Zeng M, Zhang A, Gao X, Lu X, Li Q, Liu J-M. High energy storage performances of Bi1-xSmxFe0.95Sc0.05O3 lead-free ceramics synthesized by rapid hot press sintering[J].Journal of the European Ceramic Society,2019, 39 (7): 2331-2338.

[7] Yang F, Pan Z, Ling Z, Hu D, Ding J, Li P, Liu J, Zhai J. Realizing high comprehensive energy storage performances of BNT-based ceramics for application in pulse power capacitors[J].Journal of the European Ceramic Society,2021, 41 (4): 2548-2558.

[8] Xie A, Qi H, Zuo R. Achieving Remarkable Amplification of Energy-Storage Density in Two-Step Sintered NaNbO3–SrTiO3 Antiferroelectric Capacitors through Dual Adjustment of Local Heterogeneity and Grain Scale[J].ACS Applied Materials & Interfaces,2020, 12 (17): 19467-19475.

[9] Bai X, Chen Z, Zheng P, Bai W, Zhang J, Li L, Wen F, Zheng L, Zhang Y. High recoverable energy storage density in nominal (0.67-x)BiFeO3-0.33BaTiO3-xBaBi2Nb2O9 lead-free composite ceramics[J].Ceramics International, 2021, 47 (16): 23116-23123.

[10] Hu D, Pan Z, Tan X, Yang F, Ding J, Zhang X, Li P, Liu J, Zhai J, Pan H. Optimization the energy density and efficiency of BaTiO3-based ceramics for capacitor applications[J].Chemical Engineering Journal,2021, 409: 127375.

[11] Hu Q, Tian Y, Zhu Q, Bian J, Jin L, Du H, Alikin D O, Shur V Y, Feng Y, Xu Z, Wei X. Achieve ultrahigh energy storage performance in BaTiO3–Bi(Mg1/2Ti1/2)O3 relaxor ferroelectric ceramics via nano-scale polarization mismatch and reconstruction[J].Nano Energy,2020, 67: 104264.

[12] Qiao X, Dizhang, Fudongniu, Mengshuchen, Bizhao, Xumeiliang, Pengfeiwei, Linglingchao, Xiaolianyang, Zupei Enhanced energy density and thermal stability in relaxor ferroelectric Bi0.5Na0.5TiO3-Sr0.7Bi0.2TiO3 ceramics[J].Journal of the European Ceramic Society,2019, 39 (15).

[13] Qu N, Du H, Hao X. A new strategy to realize high comprehensive energy storage properties in lead-free bulk ceramics[J].Journal of Materials Chemistry C,2019, 7 (26): 7993-8002.

[14] Murtaza T, Salmani I A, Ali J, Khan M S. Structural, electrical and magnetic study of multiferroic Bi1 - xNdxFeO3[J].Journal of Materials Science: Materials in Electronics,2018, 29 (6): 5110-5115.

[15] Li Q, Ji S, Wang D, Zhu J, Li L, Wang W, Zeng M, Hou Z, Gao X, Lu X, Li Q, Liu J-M. Simultaneously enhanced energy storage density and efficiency in novel BiFeO3-based lead-free ceramic capacitors[J].Journal of the European Ceramic Society,2021, 41 (1): 387-393.

[16] Zhu L-F, Lei X-W, Zhao L, Hussain M I, Zhao G-Z, Zhang B-P. Phase structure and energy storage performance for BiFeO3–BaTiO3 based lead-free ferroelectric ceramics[J].Ceramics International,2019, 45 (16): 20266-20275.

[17] Liu N, Liang R, Zhou Z, Dong X. Designing lead-free bismuth ferrite-based ceramics learning from relaxor ferroelectric behavior for simultaneous high energy density and efficiency under low electric field[J].Journal of Materials Chemistry C,2018, 6 (38): 10211-10217.

[18] Wang D, Khesro A, Murakami S, Feteira A, Zhao Q, Reaney I M. Temperature dependent, large electromechanical strain in Nd-doped BiFeO3-BaTiO3 lead-free ceramics[J].Journal of the European Ceramic Society,2017, 37 (4): 1857-1860.

[19] Yang D, Gao J, Shu L, Liu Y-X, Yu J, Zhang Y, Wang X, Zhang B-P, Li J-F. Lead-free antiferroelectric niobates AgNbO3 and NaNbO3 for energy storage applications[J].Journal of Materials Chemistry A,2020, 8 (45): 23724-23737.

[20] Jiang J, Meng X, Li L, Guo S, Huang M, Zhang J, Wang J, Hao X, Zhu H, Zhang S-T. Ultrahigh energy storage density in lead-free relaxor antiferroelectric ceramics via domain engineering[J].Energy Storage Materials,2021, 43: 383-390.

[21] Xie H, Du H, Liu L, Kou Q, Xu J, Sun Y, Lv R, Chang Y, Wang D. Enhanced energy storage properties under low electric fields in (Bi0.5Na0.5)TiO3-based relaxor ferroelectrics via a synergistic optimization strategy[J].Chemical Engineering Journal,2022, 450: 138432.

[22] Zhao X, Bai W, Ding Y, Wang L, Wu S, Zheng P, Li P, Zhai J. Tailoring high energy density with superior stability under low electric field in novel (Bi0.5Na0.5)TiO3-based relaxor ferroelectric ceramics[J].Journal of the European Ceramic Society,2020, 40 (13): 4475-4486.

[23] Harizanova R, Bocker C, Avdeev G, Slavov S, Costa L C, Avramova I, Rüssel C. Microstructure and electrical conduction of iron-doped barium titanate glass-ceramics[J].Journal of Non-Crystalline Solids,2021, 560: 120711.

[24] Zheng R, Zhou X, Yang Y, Wu Q, Lv P, Yu K, Wei W. Effects of heat treatment on Na-ion conductivity and conduction pathways of fluorphosphate glass-ceramics[J].Journal of Non-Crystalline Solids,2017, 471: 280-285.

[25] Zhang L, Pu Y, Chen M, Peng X, Wang B, Shang J. Design strategies of perovskite energy-storage dielectrics for next-generation capacitors[J].Journal of the European Ceramic Society,2023, 43 (14): 5713-5747.

[26] Yan F, Huang K, Jiang T, Zhou X, Shi Y, Ge G, Shen B, Zhai J. Significantly enhanced energy storage density and efficiency of BNT-based perovskite ceramics via A-site defect engineering[J].Energy Storage Materials,2020, 30: 392-400.

[27] Wang H, Jiang X, Liu X, Yang R, Yang Y, Zheng Q, Kwok K W, Lin D. An effective approach to achieve high energy storage density and efficiency in BNT-based ceramics by doping AgNbO3[J].Dalton Transactions,2019, 48 (48): 17864-17873.

[28] Yang H, Qi H, Zuo R. Enhanced breakdown strength and energy storage density in a new BiFeO3-based ternary lead-free relaxor ferroelectric ceramic[J].Journal of the European Ceramic Society,2019, 39 (8): 2673-2679.

[29] Xu R, Xu Z, Feng Y, Wei X, Tian J, Huang D. Evaluation of discharge energy density of antiferroelectric ceramics for pulse capacitors[J].Applied Physics Letters,2016, 109 (3).

[30] Zheng D, Zuo R. Enhanced energy storage properties in La(Mg1/2Ti1/2)O3-modified BiFeO3-BaTiO3 lead-free relaxor ferroelectric ceramics within a wide temperature range[J].Journal of the European Ceramic Society,2017, 37 (1): 413-418.

[31] Xu W H, Tang Y D, Yao H Y, Zhang Y H J C J O P S. Dipolar Glass Polymers for Capacitive Energy Storage at Room Temperatures and Elevated Temperatures[J],2022, 40 (7): 711-725.

[32] Cui T, Zhang J, Guo J, Li X, Guo S, Huan Y, Wang J, S.-T. Z, Wang Y. Outstanding comprehensive energy storage performance in lead-free BiFeO3-based relaxor ferroelectric ceramics by multiple optimization design[J].Acta materialia,2022.